Supporting information

π-extended regioisomeric dithienoacenes fused pyrenes: structures, properties, and application in field-effect transistors

Bin Lu,[a] Shiqian Zhang,[a] Dong Liu,[a] Wendong Jin,[a] Dalin Li,[a] Zhiqiang Liu* [a] and Tao He* [a,b]

[a] State Key Laboratory of Crystal Materials and Institute of Crystal Materials, Shandong University, Jinan 250100, China.
[b] Shenzhen Research Institute of Shandong University, Shenzhen 518057, China.
E-mail: zqliu@sdu.edu.cn; the@sdu.edu.cn

Table of Contents

1. Experimental details

Growth of single crystals: Several tens of micrometer-sized PDTAs single crystals were grown by sublimation in-air on the OTS-modified Si/SiO_2 substrate. The detailed steps are as follows: 100 μL PDTA in $CHCl_3$ (1 mg/mL) were drop cast onto Si/SiO_2 substrate. A homogeneous-dispersed thin film was formed with solvent evaporation. After that, it was heated at a temperature of 200 ℃ for 5-20 min. The organic PDTAs molecules underwent sublimation and subsequently deposited as crystalline plates on the surface of the opposing substrate. The separation between two substrates is about 1 mm. The thickness and size of the crystals can be controlled by adjusting the heated time and consumption of PDTAs material.

Device fabrication: Bottom-gate and top-contact device geometry was employed for both single crystal and thin film FETs. 40-nm-thick PDTA films were deposited onto Si/SiO_2 substrates at 10^{-5} Pa with a rate of 0.2−0.3 $Å s^{-1}$. The heavily doped Si was used as gate electrodes. For source and drain electrodes, 50 nm thick Au was patterned on the active layer by vacuum evaporation through a shadow mask. PDTA single crystal FETs have a fixed channel length (L) of 30 μm, whereas the width varies according to the actual width of the crystals.

X-ray spectroscopy: Single-crystal and film of PDTAs X-ray data were collected on a Bruker D8 Advance X-ray diffractometer with Cu Kα irradiation and λ = 1.54 Å. A continuous scan was used with a scan range of 5°–30°, step size set to 0.01° and a scan speed of 10°/min.

Atomic force microscopy: All thickness and surface morphology of single crystal and film measurements were performed with Oxford Jupiter AFM at ambient conditions in tapping mode.

UV-visible absorption spectra: A UV-visible absorption Cary 5000 spectrometer was used to determine the absorption edge and the corresponding optical band gaps for PDTA solid films and solution (10^{-5} M with hexane solution) under ambient conditions.

2. Synthetic details

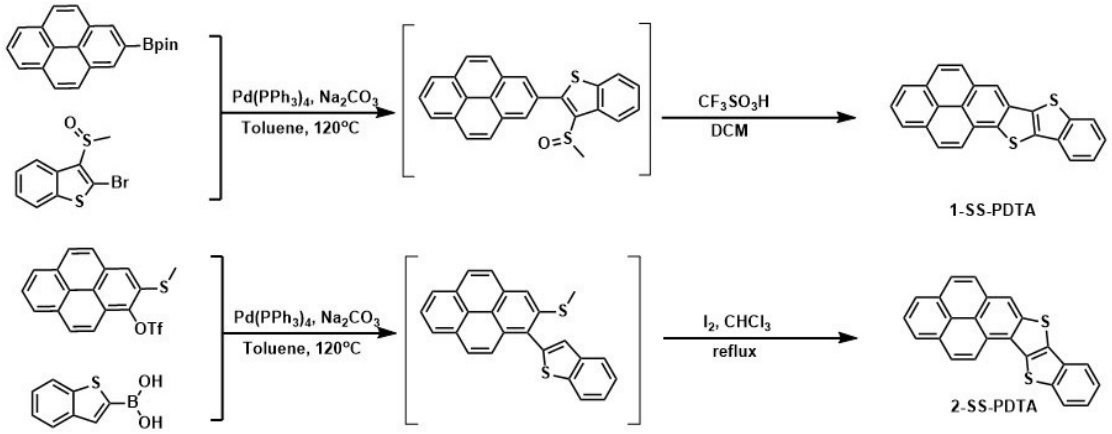

Scheme S1. Synthetic approach to regioisomers of 1-SS-PDTA and 2-SS-PDTA.

1-SS-PDTA

2-Bpin-pyrene[1] (0.300 g, 0.91 mmol) and 2-bromo-3-thiomethylsulfinylbenzo[b]thiophene[2] (0.302 g, 1.10 mmol) were dissolved in 20 mL toluene/H_2O (10:1) mixed solvent under an Ar atmosphere, and then catalysts tetrakis(triphenylphosphine)palladium (0.046 g, 0.04 mmol) and Na_2CO_3 (0.151 g, 1.09 mmol) were added and the reaction was refluxed at 120 °C for 24 hours. After the reaction was quenched, it was extracted three times with 20 mL CH_2Cl_2, and the combined organic layers were dried with anhydrous $MgSO_4$, filtered, spun-dried in vacuum, and operated over the column with petroleum ether/ethyl acetate (4:1) as the eluent to obtain 0.334 g of light yellow solid of precursor compound (2-(3-Thiomethylsulfinyl-benzo[b]thiophene)pyrene with 92% yield).

Then, this precursor compound (2-(3-Thiomethylsulfinyl-benzo[b]thiophene)pyrene (0.344 g, 0.87 mmol) was dissolved in 20 mL CH_2Cl_2 in a round-bottomed flask. Next, 1.50 mL trifluoromethanesulfonic acid was added with the solution turned black. The above solution was sealed and stirred at room temperature for 24 hours. The reaction was finished by slowly adding it to a mixture of 60 mL water/pyridine (8:1) and refluxed for 30 min to demethylate. After returning to room temperature, the solution was filtered and a dark red precipitate was obtained by drenching with water and ethanol. Over-column operation using petroleum ether/CH_2Cl_2 (2:1) as eluent gave 0.249 g of the final product 1-SS-PDTA as an orange-yellow powder in 78% yield.

M.p. 292°C. ^{1}H NMR (300 MHz, CDCl3) δ 8.60 (s, 1H), 8.39 (d, 1H, *J*=10.0 Hz), 8.25 (t, 2H, J_1=10.0 Hz, J_2=6.4 Hz), 8.17 (m, 2H), 8.03 (m, 4H), 7.53 (m, 1H), 7.46 (m, 1H). ^{13}C NMR (100 MHz, $CDCl_3$) δ 142.54, 137.74, 134.32, 133.36, 133.33, 131.22, 131.19, 131.04, 129.45, 128.57, 127.77, 127.33, 126.84, 125.96, 125.75, 125.44, 125.15, 125.06, 124.96, 124.16, 123.04, 121.72, 117.47 ppm. HRMS (EI): m/z[M]$^{+}$: 364.0378; calcd for $C_{24}H_{12}S_2^{+}$ 364.0380.

2-SS-PDTA

2-(methylthio)-1-OTf-pyrene (0.2g, 0.5mmol)[3] and benzo[b]thiophen-2-ylboronic acid (0.11 g, 0.6 mmol) were added to a 10ml solution of methanol: water: toluene=1:1:1. Then, $Pd(PPh_3)_4$ (10％eq), and Na_2CO_3 (0.23 g, 1.67 mmol) were added into the mixture. The mixture was then stirred at 120℃ for 24 hours. Then 30 ml of water was added to the mixture and the organic layer was separated, whereas the aqueous layer was extracted two times with 20 mL of ethyl acetate. Then, combined extracts were dried over Na_2SO_4. The solvent was evaporated to obtain reddish brown powder of precursor compound 1-(2'-benzo[b]thiophene)- 2-(methylthio)-pyrene. The product was not purified and used directly in the next step.

Compound 1-(2'-benzo[b]thiophene)-2-(methylthio)-pyrene (0.30 mmol) and iodine (1.25g, 4.93 mmol) were dissolved in 8 ml chloroform, and reacted at 70 °C (1 hour), 80 °C (1 hour) and 90 °C (22 hours).[4] Then cool to RT, it was poured into saturation sodium thiosulfate (aq), extract with DCM, dried ($MgSO_4$), concentrated in vacuum and purified by passing a silica gel column using PE/DCM (8/1) as eluent to give 0.27 g bright yellow powder in 80 % yield. M.p. 269°C. ^{1}H NMR (300 MHz, $CDCl_3$) δ 8.78 (d, 1H, *J*=12.0 Hz), 8.66 (s, 1H), 8.38 (d, 1H, *J*=12.0 Hz), 8.29 (m, 1H), 8.22 (m, 1H), 8.05 (m, 5H), 7.51 (m, 2H). ^{13}C NMR (100 MHz, $CDCl_3$) δ 142.97, 140.66, 134.08, 132.69, 132.63, 131.14, 130.61, 129.33, 128.33, 127.88, 127.65, 127.24, 125.87, 125.51, 125.35, 125.29, 125.11, 124.99, 123.79, 123.60, 122.74, 121.60, 119.85 ppm. HRMS (EI): m/z[M]$^{+}$: 364.0377; calcd for $C_{24}H_{12}S_2^{+}$ 364.0380.

3. PDTAs molecular orbitals isosurfaces and energy transitions

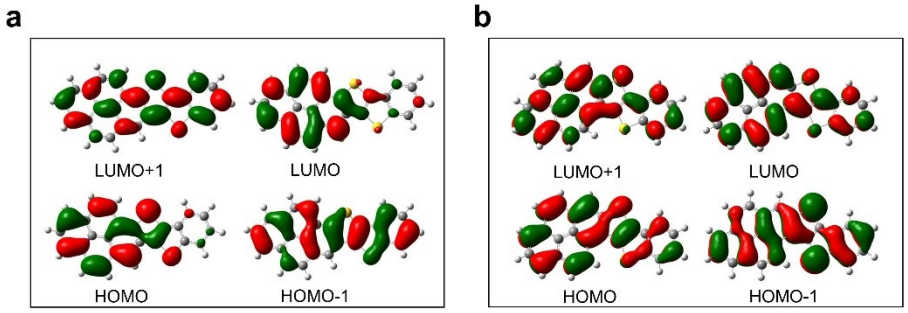

Figure S1. The isosurfaces (isovalue = 0.02 $[ea_0^{-3}]^{½}$) of selected molecular orbitals of (a)1-SS-PDTA and (b) 2-SS-PDTA, as calculated by DFT at the B3LYP/6-311G(d).

Table S1 Energy transitions of 1-SS-PDTA, calculated by TD-DFT/B3LYP/6-311G(d)

Excited State S1				
Orbital transitions	Contribution coefficient	Excitation energy (E/eV)	Excitation wavelength (λ / nm)	Oscillator strength (f)
HOMO-1 → LUMO	0.465	3.22	385.2	0.002
HOMO → LUMO	0.509			
Excited State S2				
HOMO-2→ LUMO	0.107	3.26	379.87	0.103
HOMO-1 → LUMO+1	-0.110			
HOMO→ LUMO	0.655			
HOMO → LUMO+1	0.156			
Excited State S3				
HOMO-2 → LUMO	-0.155	3.73	332.69	0.280
HOMO-1 → LUMO	0.475			
HOMO-1 → LUMO+1	-0.226			
HOMO → LUMO	0.107			
HOMO → LUMO+1	-0.392			

Table S2 Energy transitions of 2-SS-PDTA, calculated by TD-DFT/B3LYP/6-311G(d)

Excited State S1				
Orbital transitions	Contribution coefficient	Excitation energy (E/eV)	Excitation wavelength (λ / nm)	Oscillator strength (f)
HOMO → LUMO	0.688	3.02	410.61	0.607
Excited State S2				
HOMO-2 → LUMO	-0.163	3.39	365.28	0.073
HOMO-1 → LUMO	0.565			
HOMO → LUMO+1	-0.321			
HOMO →LUMO+1	-0.186			
Excited State S3				
HOMO-1 → LUMO	0.465	3.65	339.87	0.065
HOMO-1 → LUMO	0.335			
HOMO → LUMO+1	0.389			

4. X-ray crystal structure and date of PDTAs

Table S3. Crystallographic data for 1-SS-PDTA and 2-SS-PDTA compounds

Data points	1-SS-PDTA	2-SS-PDTA
Formula	$C_{24}H_{12}S_2$	$C_{24}H_{12}S_2$
Formula weight (g/mol)	364.46	364.46
Crystal system	Orthorhombic	Orthorhombic
Space group	$P2_12_12_1$	$P2_12_12_1$
Temperature (K)	301	296
a (Å)	4.3795(2)	4.5998(3)
b (Å)	13.5336(8)	13.6871(8)
c (Å)	27.4731(15)	25.8017(14)
α (°)	90	90
β (°)	90	90
γ (°)	90	90
V (Å^3)	1628.34 (15)	1624.42 (17)
Z	4	4
F (000)	752	752
ρ (g/cm^3)	1.487	1.490
μ (cm^{-1})	0.2947	0.332
Independent reflections	2959	3707
Number of parameters	202	235
C-C bond precision (Å)	0.0093	0.0074
CCDC number	2370209	2379035

5. The thicknesses of PDTAs single crystals

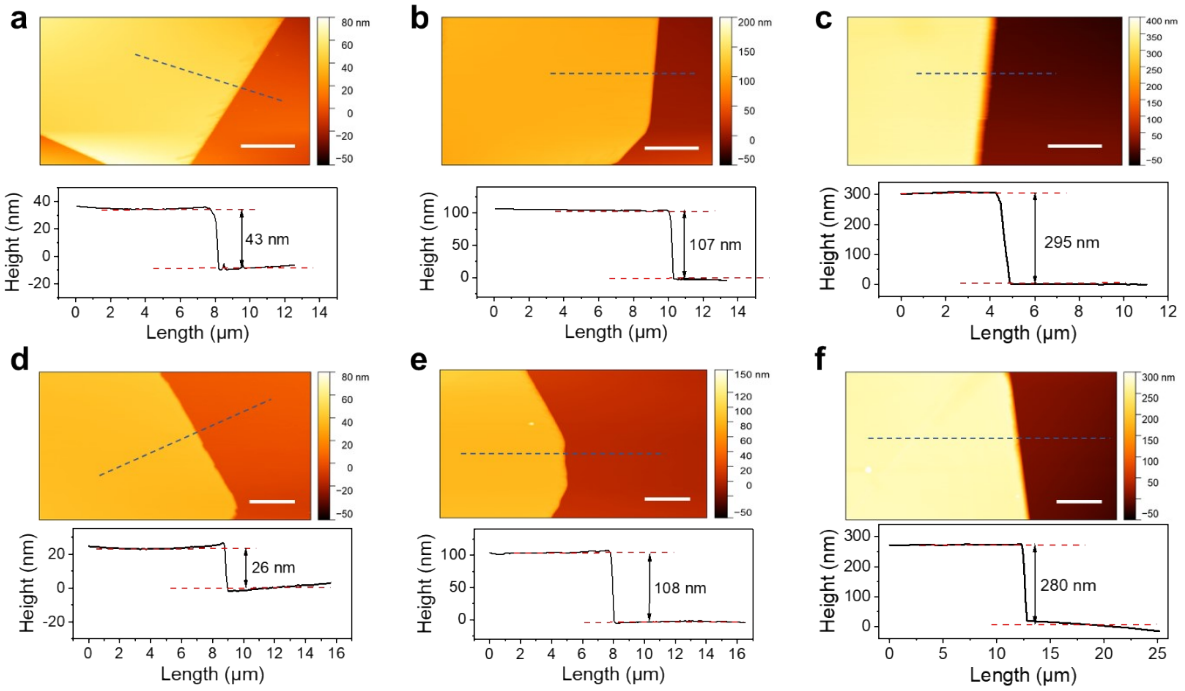

Figure S2. The AFM images of the regioisomeric PDTA single crystals with different thicknesses. AFM images of (a-c)1-SS-PDTA and (d-f) 2-SS-PDTA single crystals, respectively, as well as the corresponding height profiles along the dashed lines. The scale bars are 5 μm. The separation between the growth substrate and the source substrate was set at a constant value of 1 mm. The thickness of crystals is determined by the period of crystal growth. (a, d) Crystals with a thickness of less than 50 nm were obtained by a growth period of 5-7 minutes. (b, e) Crystals with a thickness of 100-200 nm were formed within approximately 15 minutes. (c, f) Crystals with a thickness of more than 200 nm necessitate a growth duration of 20-30 minutes.

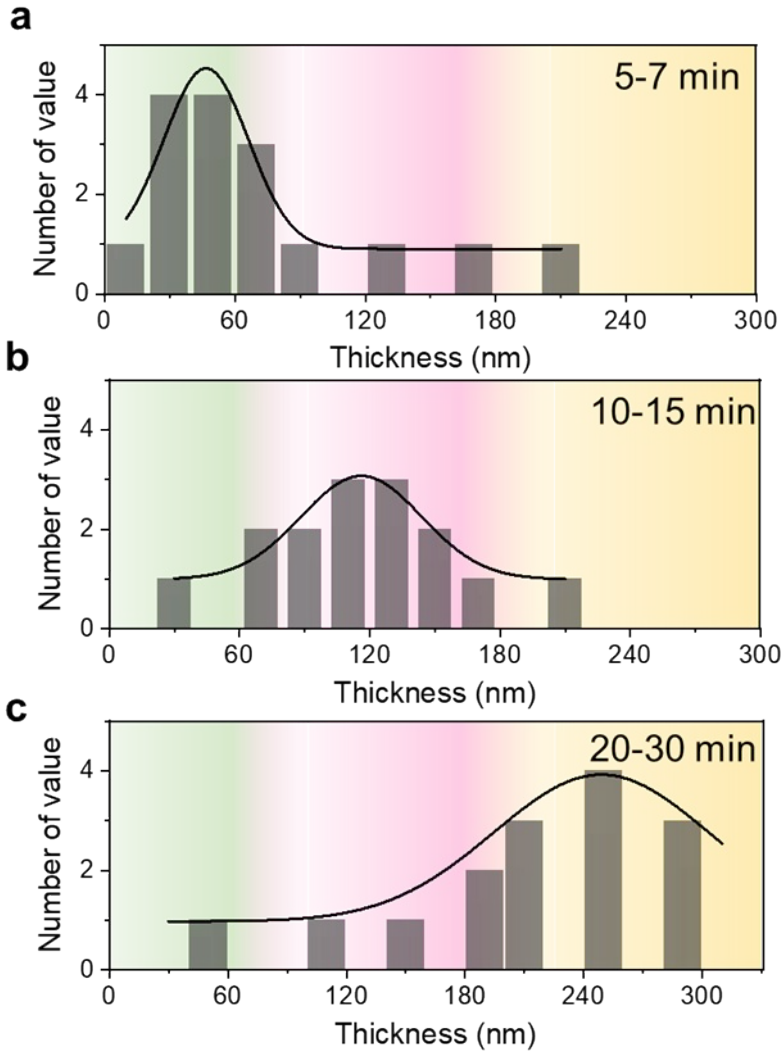

Figure S3. The thickness distribution graph of PDTA single crystals growth for (a) 5-7 min (b) 10-15 min and (c) 20-30 min.

6. OFET properties based PDTAs single crystals and thin films

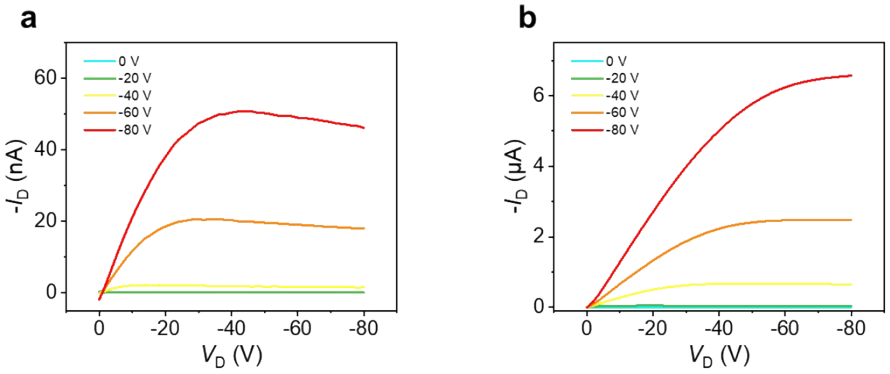

Figure S4. The output characteristics of (a) 1-SS-PDTA and (b) 2-SS-PDTA single-crystal OFETs.

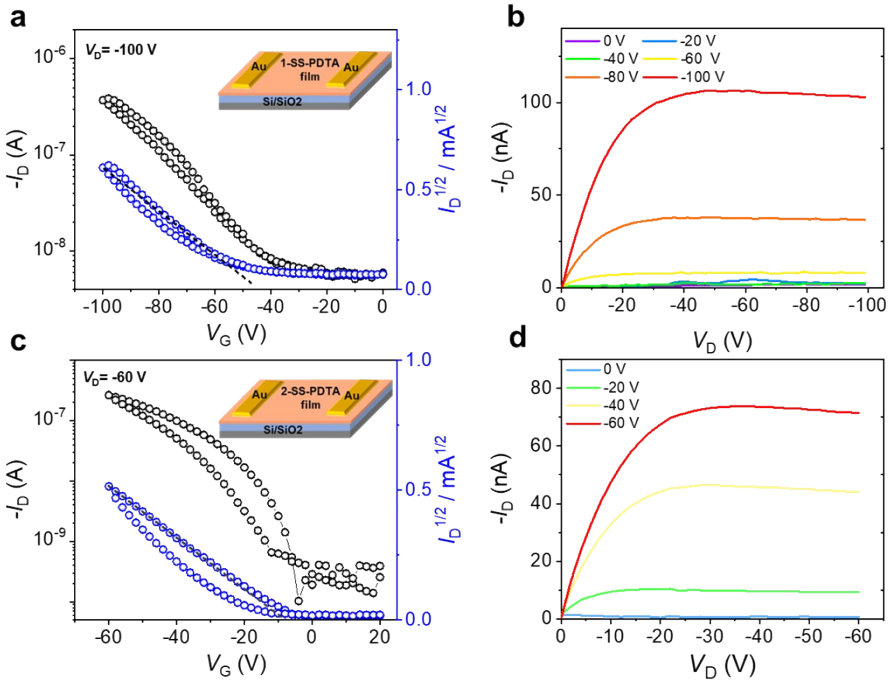

Figure S5. The transfer and output characteristics of (a, b) 1-SS-PDTA and (c, d) 2-SS-PDTA thin film FETs at room temperature.

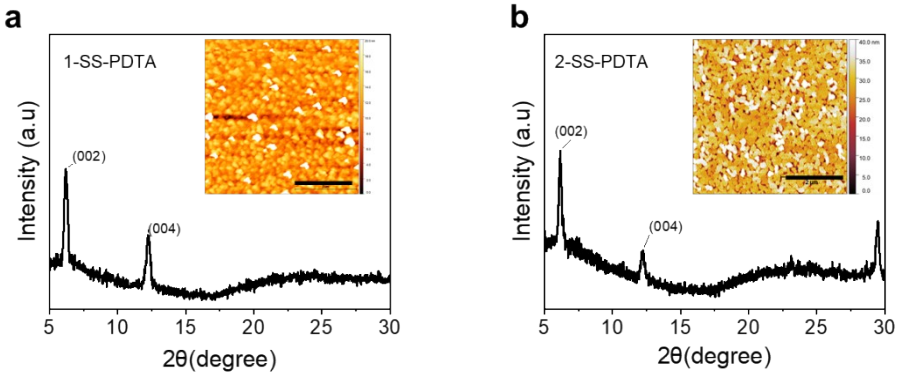

Figure S6. XRD images of vacuum-deposited (a) 1-SS-PDTA and (b) 2-SS-PDTA thin films. Insets to (a) and (b): the corresponding AFM topographies. The Scale bars are 2 μm.

7. DFT calculations of isolated molecule properties and mobility

The molecular ground-state geometry is optimized through Density Functional Theory (DFT) using the B3LYP functional and a 6-311+G(d,p) basis set. Following this, frequency calculations are performed to obtain the vibrational modes and verify that the geometry optimization has reached a local minimum. Next, Time-Dependent DFT (TD-DFT) is employed to calculate the vertical excitation energies and transition dipole moments at the optimized ground-state geometry.

Reorganization energy: The reorganization energy is then calculated by using the vibrational modes and normal mode displacement. It involves performing frequency calculations for the neutral, cationic, and anionic states of the molecules. The internal reorganization energy (λ) is determined by calculating the energy required to reorganize the molecular structure during the charge transfer process.[5] Specifically, it is the sum of the relaxation energies of the molecule in its charged and neutral states. The reorganization energy is obtained from the following expression.[6]

$$\lambda = \frac{(E_1 - E_2)}{2} + \frac{(E_3 - E_4)}{2} \tag{1}$$

where E_1, E_2, E_3, and E_4 are the energies of the neutral molecule in the charged geometry, the neutral molecule in the neutral geometry, the charged molecule in the neutral geometry and the charged molecule in the neutral geometry, respectively.

Transfer integrals: Transfer integrals (V) between neighboring molecules are conducted by constructing dimers of the molecules and performing single-point energy calculations. The transfer integral is calculated using the energy splitting in the dimer's highest occupied molecular orbitals (HOMOs).[7] The transfer integral is given by:

$$V = \frac{E_{HOMO}^{dimer} - E_{HOMO}^{monomer}}{2} \tag{2}$$

where E_{HOMO}^{dimer} is the energy of the dimer's HOMO, and $E_{HOMO}^{monomer}$ is the energy of the monomer's HOMO.

Mobility: Kinetic Monte Carlo (KMC) simulations are conducted to model the charge transport process.[8, 9] The hopping rates for charge carriers are derived from Marcus–

Levich–Jortner (M−J−L) equation,[10, 11] which provides an expression for the rate constant as:

$$k = \frac{2\pi}{\hbar} V^2 \frac{1}{\sqrt{4\pi\lambda k_B T}} \sum_n e^{-S_M} \frac{S_M{}^n}{n!} exp[-\frac{(\Delta G + \lambda + n\hbar\omega_M)^2}{4\lambda k_B T}] \quad (3)$$

where ΔG is the change in Gibbs free energy; k_B is the Boltzmann constant; T is the temperature; ω_M represents the average value of high-frequency (>1000 cm^{-1}) intramolecular vibrational modes; S_M is the effective Huang–Rhys factor; $\hbar$ is the reduced Planck constant. The calculation details of ω_M and S_M are given in the reference paper.[12]

The KMC algorithm tracks the movement of charge carriers through the molecular lattice, considering the calculated hopping rates. Random charge hopping events are generated, and the trajectory of each charge carrier is simulated over time. The diffusion coefficient (D) of the charge carriers is calculated from the mean-square displacement (MSD) of the carriers over time, using the relation:

$$D = \frac{< MSD >}{2d\Delta t} \quad (4)$$

Where d is the dimensionality of the system, and Δt is the time interval. Finally, the charge carrier mobility (μ) is obtained using the Einstein relation:

$$\mu = \frac{eD}{k_B T} \quad (5)$$

where e is the elementary charge.

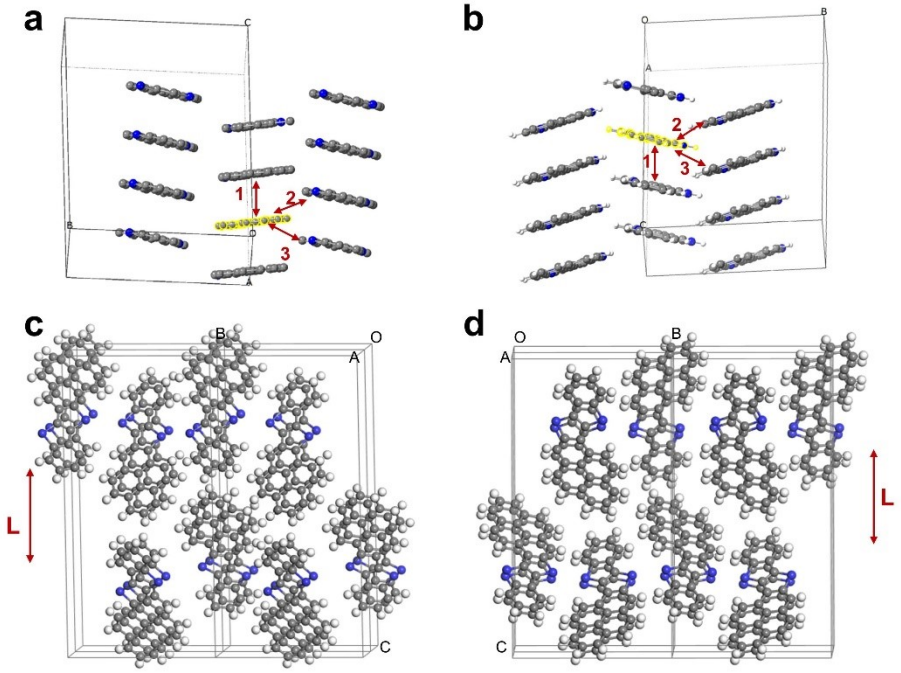

Figure S7. Transfer integrals are computed for the nearest neighbor pairs. (a, b) Three near-neighbor intermolecular interactions (configuration 1, configuration 2, and configuration 3) of (a) 1-SS-PDTA and (b) 2-SS-PDTA in the *ab*-plane, respectively. (c, d) Longitudinal (L) near-neighbor intermolecular interactions along the c-axis for (c) 1-SS-PDTA and (d) 2-SS-PDTA.

Table S4. Calculated reorganization energies and transfer integrals of the two PDTA regioisomers.

	1-SS-PDTA	2-SS-PDTA
Reorganization energies	118.29 meV	167.09 meV
Transfer integrals (configuration 1)	77.683 meV	90.719 meV
Transfer integrals (configuration 2)	7.915 meV	2.956 meV
Transfer integrals (configuration 3)	1.158 meV	0.311 meV

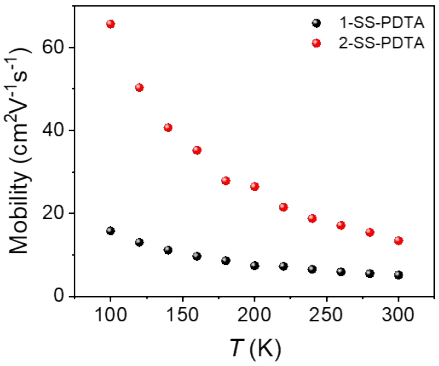

Figure S8. Calculated the temperature dependence hole mobility of the two PDTA regioisomers. 2-SS-PDTA exhibits a more pronounced temperature-dependent behavior in terms of band-like charge transport.

8. The fluorescence emission spectra of PDTAs

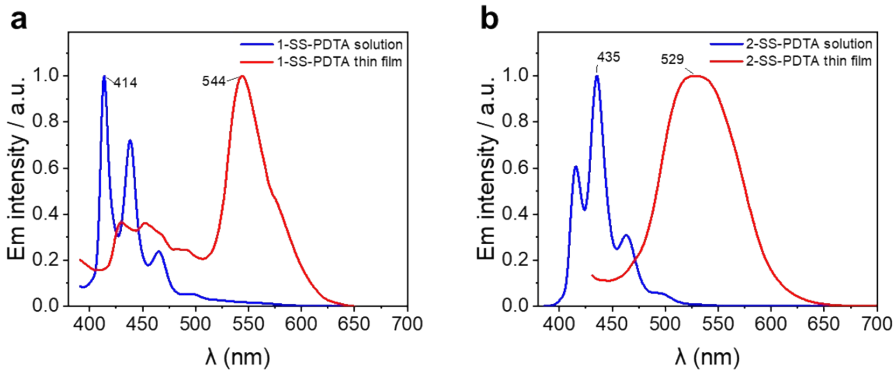

Figure S9. The fluorescence emission spectra of (a) 1-SS-PDTA and (b) 2-SS-PDTA in solution (10^{-5} M with hexane solution) and thin films. The red shift in the thin film state is caused by the formation of J-aggregates. Emission maxima were observed at 544 nm and 529 nm for 1-SS-PDTA and 2-SS-PDTA thin films, respectively.

9. Thermal stability and air stability of PDTAs devices

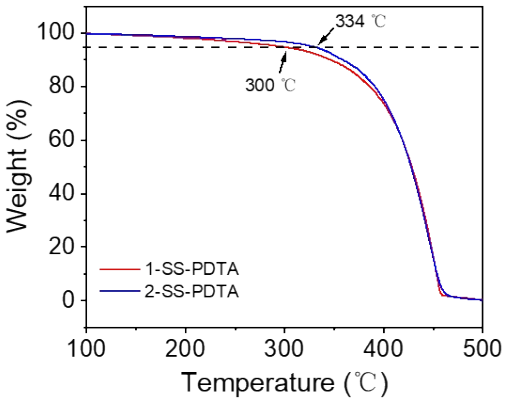

Figure S10. Thermal analysis measurements (TGA) of 1-SS-PDTA and 2-SS-PDTA. TGA tests of the two PDTAs were performed under N_2 protection. 3 mg powders were heated from 30℃ to 500°C at a rate of 10 °C/min. The thermal decomposition temperatures (at 5% weight loss) of 2-SS-PDTA were 334°C, larger than that of 1-SS-PDTA (300°C). This is possible attribute to 2-SS-PDTA has stronger intermolecular interactions. Therefore, 2-SS-PDTA molecule have better thermal stability and air stability.

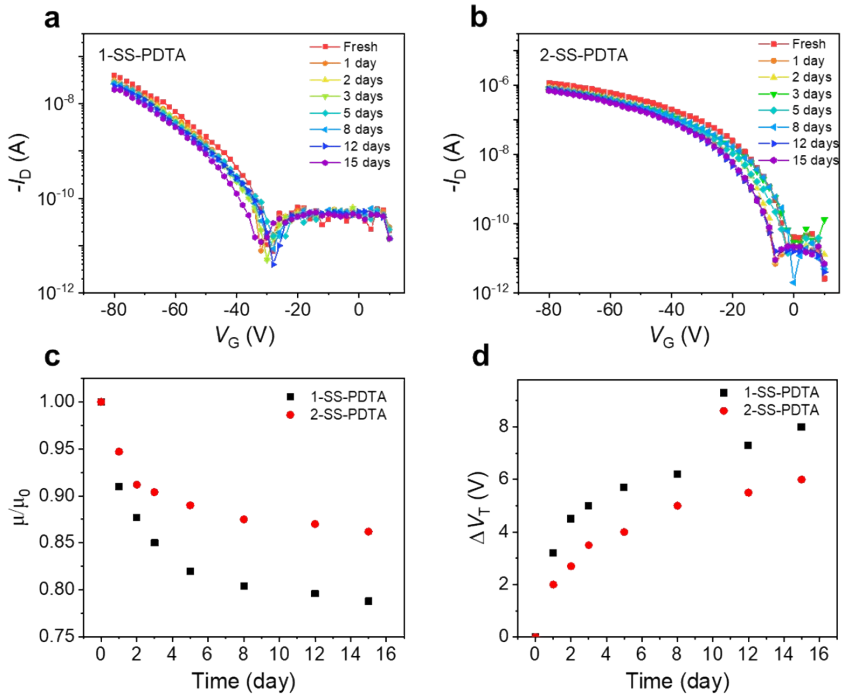

Figure S11. Air stability of PDTAs single crystal FETs by storing for 15 days in ambient.

10. ^{1}H and ^{13}C NMR spectra for the products

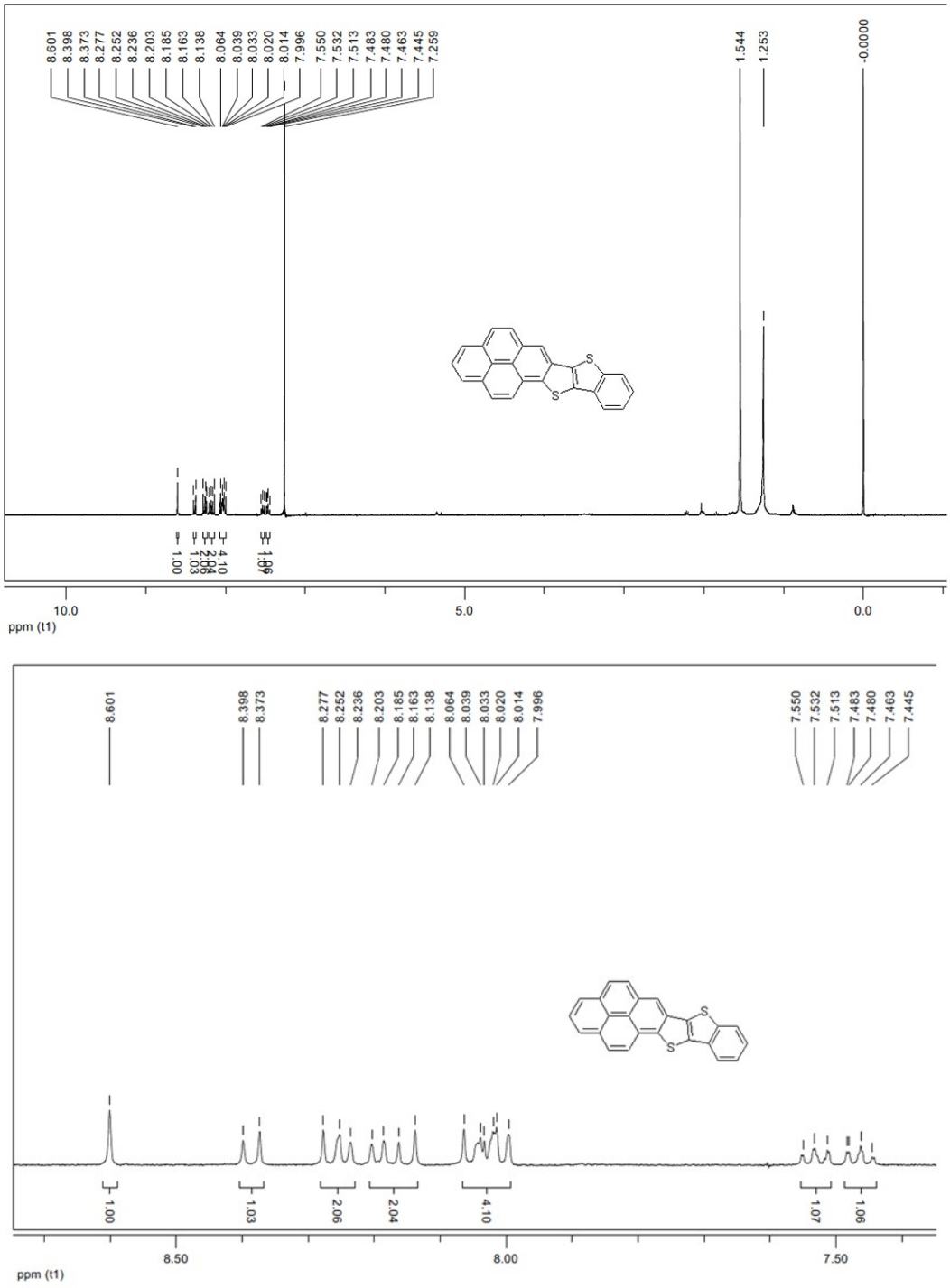

Figure S12. ^{1}H NMR spectra of 1-SS-PDTA measured in $CDCl_3$ (inset shows the spectral region for aromatic protons).

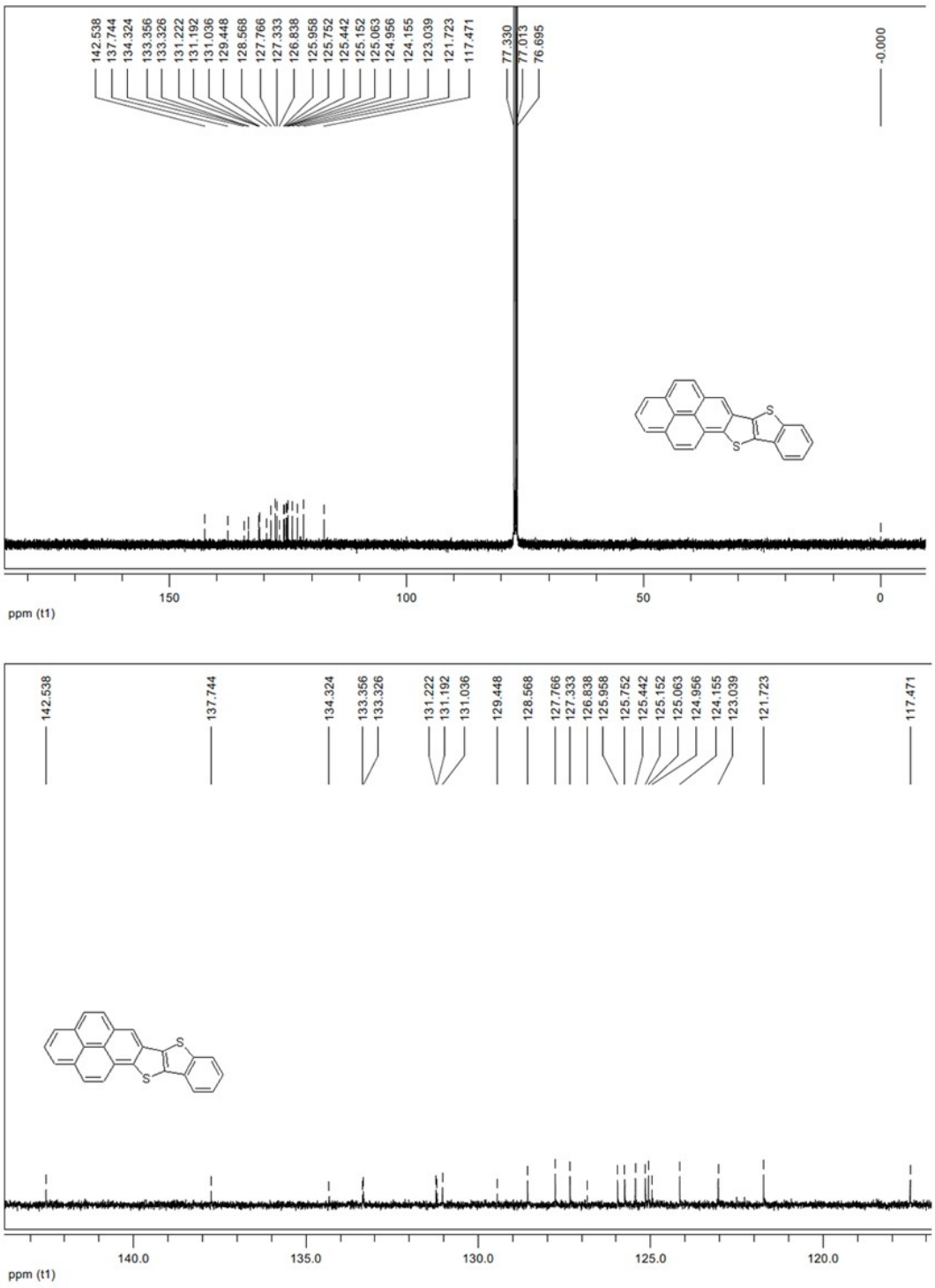

Figure S13. ^{13}C NMR spectra of 1-SS-PDTA measured in $CDCl_3$.

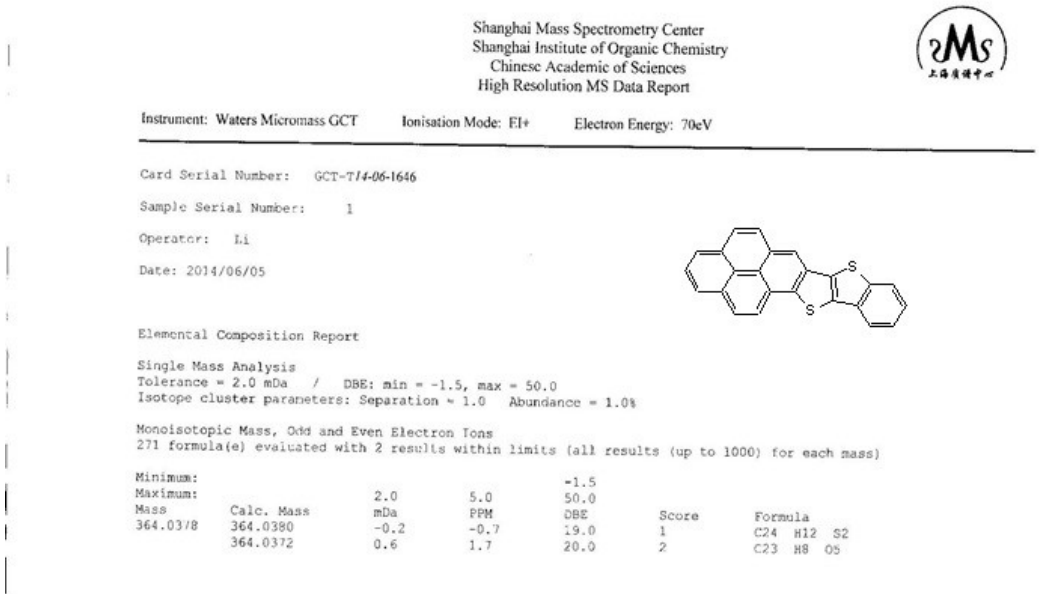

Shanghai Mass Spectrometry Center
Shanghai Institute of Organic Chemistry
Chinese Academic of Sciences
High Resolution MS Data Report

Instrument: Waters Micromass GCT Ionisation Mode: EI+ Electron Energy: 70eV

Card Serial Number: GCT-T*14-06-1646*

Sample Serial Number: 1

Operator: Li

Date: 2014/06/05

Elemental Composition Report

Single Mass Analysis
Tolerance = 2.0 mDa / DBE: min = -1.5, max = 50.0
Isotope cluster parameters: Separation = 1.0 Abundance = 1.0%

Monoisotopic Mass, Odd and Even Electron Ions
271 formula(e) evaluated with 2 results within limits (all results (up to 1000) for each mass)

Minimum:				-1.5		
Maximum:		2.0	5.0	50.0		
Mass	Calc. Mass	mDa	PPM	DBE	Score	Formula
364.0378	364.0380	-0.2	-0.7	19.0	1	C24 H12 S2
	364.0372	0.6	1.7	20.0	2	C23 H8 O5

Figure S14. HR-MS of 1-SS-PDTA.

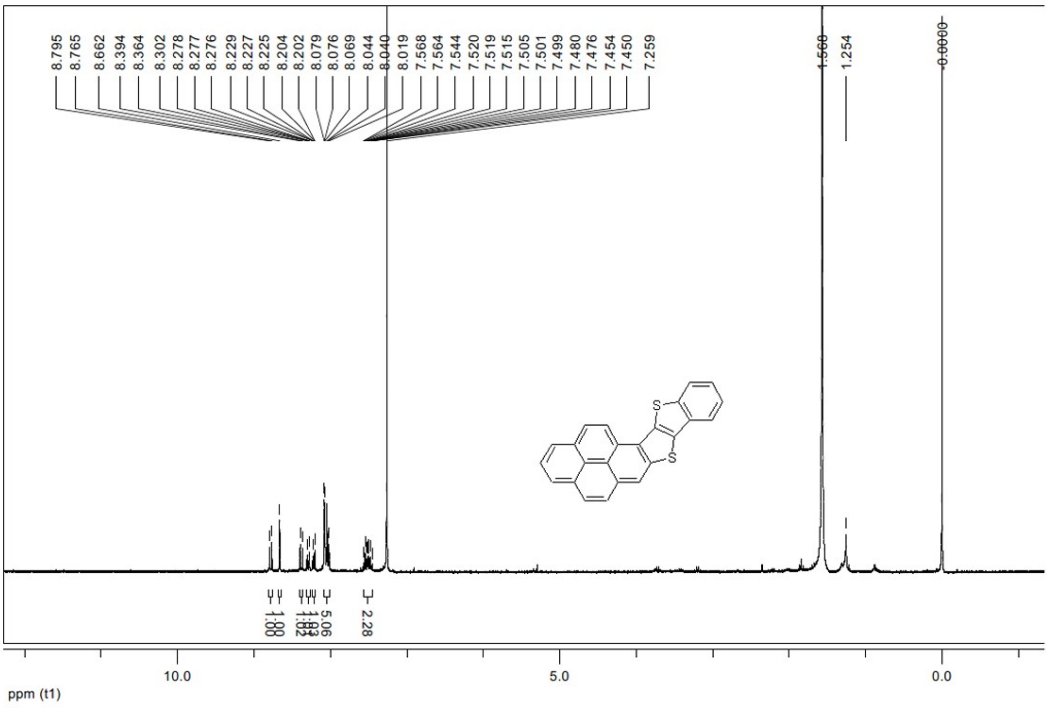

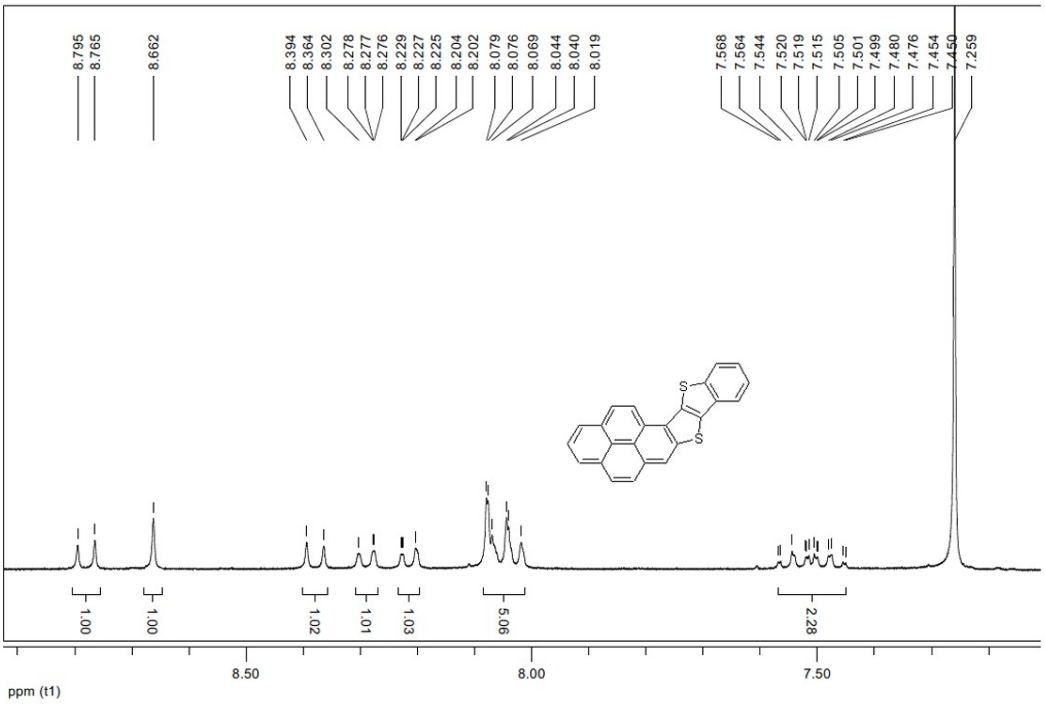

Figure S15. ^{1}H NMR spectra of 2-SS-PDTA measured in $CDCl_3$ (inset shows the spectral region for aromatic protons).

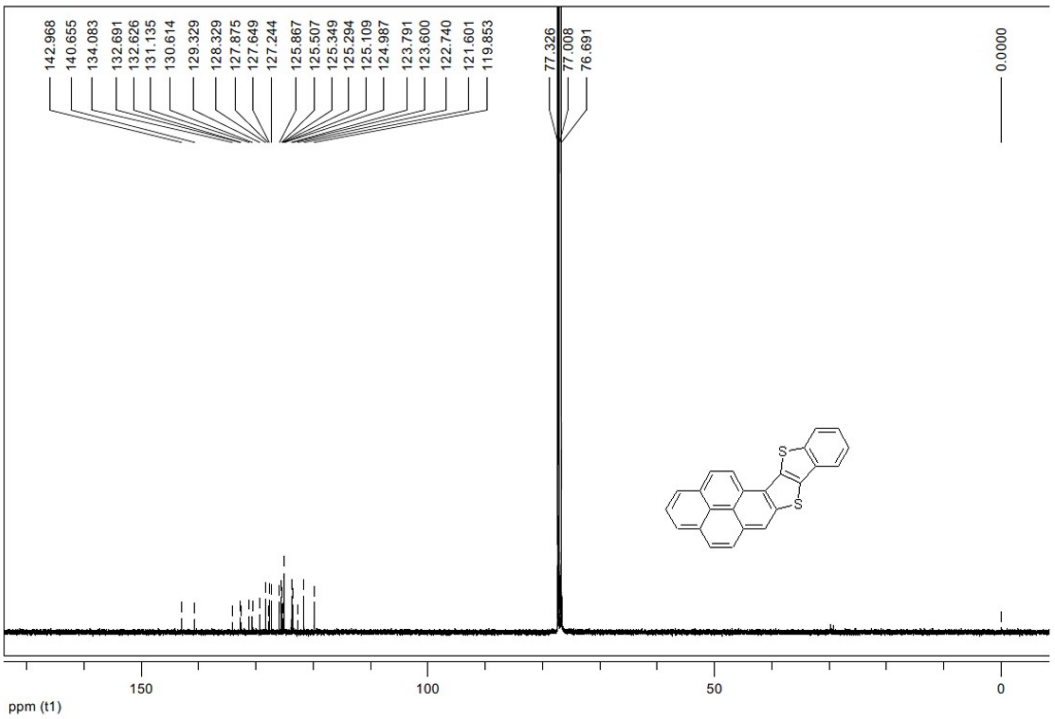

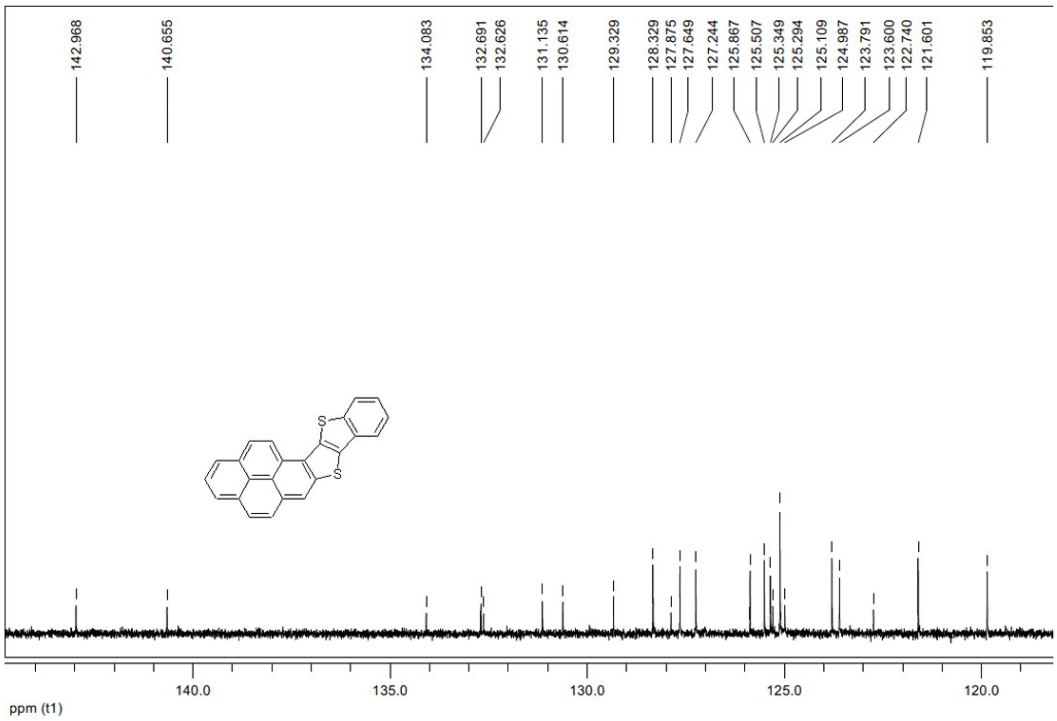

Figure S16. ^{13}C NMR spectra of 2-SS-PDTA measured in $CDCl_3$.

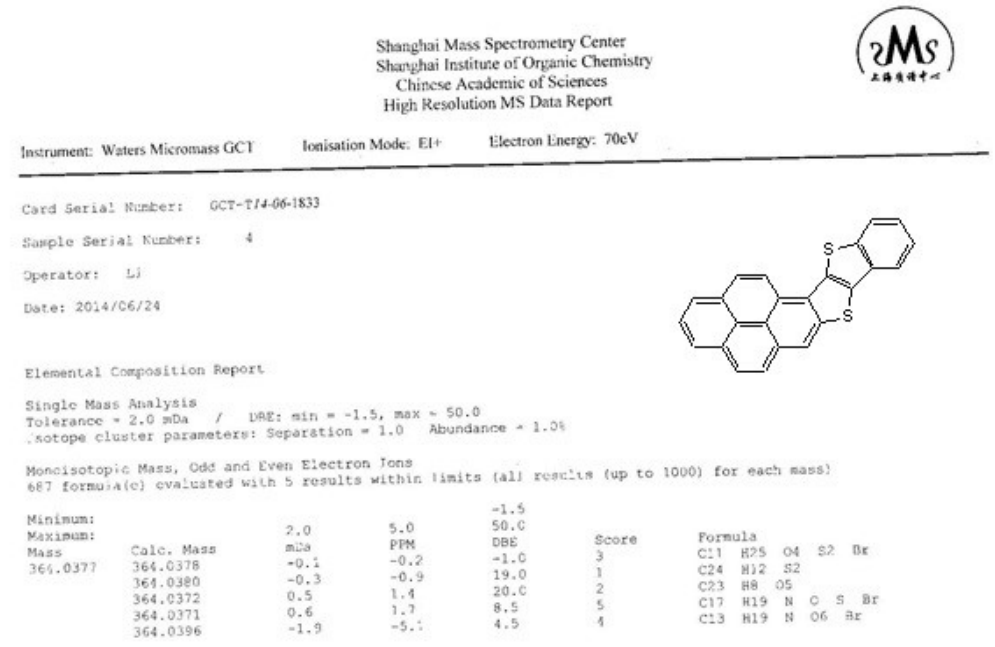

Shanghai Mass Spectrometry Center
Shanghai Institute of Organic Chemistry
Chinese Academic of Sciences
High Resolution MS Data Report

Instrument: Waters Micromass GCT Ionisation Mode: EI+ Electron Energy: 70eV

Card Serial Number: GCT-T14-06-1833

Sample Serial Number: 4

Operator: LJ

Date: 2014/06/24

Elemental Composition Report

Single Mass Analysis
Tolerance = 2.0 mDa / DBE: min = -1.5, max = 50.0
Isotope cluster parameters: Separation = 1.0 Abundance = 1.0%

Monoisotopic Mass, Odd and Even Electron Ions
687 formula(e) evaluated with 5 results within limits (all results (up to 1000) for each mass)

Minimum:				-1.5		
Maximum:		2.0	5.0	50.0		
Mass	Calc. Mass	mDa	PPM	DBE	Score	Formula
364.0377	364.0378	-0.1	-0.2	-1.0	3	C11 H7 S 04 S2 Br
	364.0380	-0.3	-0.9	19.0	1	C24 H12 S2
	364.0372	0.5	1.4	20.0	2	C23 H8 O5
	364.0371	0.6	1.7	8.5	5	C17 H19 N O S Br
	364.0396	-1.9	-5.1	4.5	4	C13 H19 N O6 Br

Figure S17. HR-MS of 2-SS-PDTA.

References

1. A. G. Crawford, Z. Liu, I. A. Mkhalid, M. H. Thibault, N. Schwarz, G. Alcaraz, A. Steffen, J. C. Collings, A. S. Batsanov, J. A. Howard and T. B. Marder, Synthesis of 2- and 2,7-functionalized pyrene derivatives: an application of selective C-H borylation, *Chemistry*, 2012, **18**, 5022-5035.
2. Y. Xiong, X. Qiao, H. Wu, Q. Huang, Q. Wu, J. Li, X. Gao and H. Li, Syntheses and properties of nine-ring-fused linear thienoacenes, *J. Org. Chem.*, 2014, **79**, 1138-1144.
3. S. Zhang, X. Qiao, Y. Chen, Y. Wang, R. M. Edkins, Z. Liu, H. Li and Q. Fang, Synthesis, structure, and opto-electronic properties of regioisomeric pyrene-thienoacenes, *Org.Lett*, 2014, **16**, 342-345.
4. S. Zhang, Z. Liu and Q. Fang, Synthesis, Structures, and Optoelectronic Properties of Pyrene-Fused Thioxanthenes, *Org.Lett*, 2017, **19**, 1382-1385.
5. Q. Peng, Y. P. Yi, Z. G. Shuai and J. S. Shao, Excited state radiationless decay process with Duschinsky rotation effect: Formalism and implementation, *J. Chem. Phys.*, 2007, **126**, 114302.
6. Y. Niu, Q. Peng and Z. Shuai, Promoting-mode free formalism for excited state radiationless decay process with Duschinsky rotation effect, *SCI CHINA SER B*, 2008, **51**, 1153-1158.
7. Q. Peng, Y. Niu, Q. Shi, X. Gao and Z. Shuai, Correlation Function Formalism for Triplet Excited State Decay: Combined Spin-Orbit and Nonadiabatic Couplings, *J. Chem. Theory Comput.*, 2013, **9**, 1132-1143.
8. D. T. Gillespie, A general method for numerically simulating the stochastic time evolution of coupled chemical reactions, *J. Comput. Phys.*, 1976, **22**, 403-434.
9. A. B. Bortz, M. H. Kalos and J. L. Lebowitz, A new algorithm for Monte Carlo simulation of Ising spin systems, *J. Comput. Phys.*, 1975, **17**, 10-18.
10. P. F. Barbara, T. J. Meyer and M. A. Ratner, Contemporary issues in electron transfer research, *J. Comput. Phys.*, 1996, **100**, 13148-13168.
11. J. Jortner, Temperature dependent activation energy for electron transfer between biological molecules, *J. Comput. Phys.*, 1976, **64**, 4860-4867.
12. A. Ito and T. J. Meyer, The Golden Rule. Application for fun and profit in electron transfer, energy transfer, and excited-state decay, *PCCP*, 2012, **14**, 13731-13745.